# Online Parameter Identification for Supercapacitor State-of-Health Diagnosis for Vehicular Applications

Asmae El Mejdoubi, *Member, IEEE*, Hicham Chaoui, *Senior Member, IEEE*, Hamid Gualous, *Member, IEEE*, and Jalal Sabor

***Abstract*—In power electronic applications, aging of the electric double layer capacitors (EDLCs) is considered as a serious issue since it may lead to failure. Their degradation is usually evaluated by an increase of the internal resistance or a decrease of the equivalent capacitance. These aging indicators have a good correlation with the supercapacitor's state-of-health (SoH). Generally, SoH is measured by electrochemical impedance spectroscopy (EIS). However, this technique must be performed offline and requires interruption of the system's operation. In this paper, a sliding mode observer is designed to estimate online the EDLC's aging indicators. Unlike several online estimators, the supercapacitor's parameters are considered as a nonlinear random distribution with external noises which yields accurate estimation. In addition, the relationship between the capacitance and the bias voltage is considered to be nonlinear. Lyapunov stability analysis is also provided. The proposed approach is validated experimentally using a standardized dynamic current profile. Furthermore, comparison against EIS is carried out for different aging phases and under different environmental temperature conditions.**

***Index Terms*—Aging diagnosis, aging parameters, capacitance, electric double-layer capacitor, resistance, sliding mode observer, supercapacitors.**

## I. Introduction

SUPERCAPACITORS, also called electric double layer capacitors (EDLCs), are buffer storage components in electrical energy systems [1]. They are more suitable for providing and absorbing instantaneous power pulses as in acceleration and braking of electric vehicles [2]. Despite their benefits, these components do not have the anticipated economic growth worldwide because of their high price. In addition, these components may contain acetonitrile, which is flammable and explosive. Finally, the voltage per cell is limited to 3 V, which makes necessary the series connection of a large number of components [3]. This series arrangement causes an imbalance between the voltages across each component, which has the effect of accelerating the supercapacitors aging and thus reducing their lifespan [4].

The integration of this storage device in vehicular applications requires a profound analysis of their aging mechanisms with the aim of improving safety via predictive maintenance processes [5]. Indeed, the supercapacitors' aging in electric vehicles results in an increase of the impedance, which leads to a loss of power and storage capacity [6]. The aging mechanisms occur not only during the usage of the EDLCs (cycling aging) but also during rest phases (calendar aging) [1], [7].

Optimal energy utilization and minimization of degradation effects are among the typical challenges to be faced. Therefore, online lifetime diagnostic of supercapacitors is required to guarantee high performance and their early failure prediction. This diagnosis model would be able to identify the aging indicators, which lead to an online state-of-health (SoH) estimation for supercapacitors. Conventional diagnosis techniques such as electrochemical impedance spectroscopy (EIS) or alternating current signal injection are known for their simplicity. For EDLCs, the EIS is usually performed by measuring the current through the cell after applying an ac bias voltage to a supercapacitor. The obtained ac current signal is analyzed as a sum of sinusoidal functions (Fourier series). As for the alternating current signal injection method, it consists of applying an alternating sinusoidal excitation current to a supercapacitor to measure its voltage response during charging/discharging cycles [8]. However, these diagnosis techniques often require additional hardware and costly analysis instrumentation.

Several online supercapacitors diagnosis model have been reported in the literature in various applications. Nadeau *et al*. [9] present a supercapacitor state-of-charge estimation for a solar application using Kalman filter. Three-branch supercapacitor equivalent circuit has been chosen to model the supercapacitor considering the *RC* circuit parameters as constants with the aging time. In addition, Chiang *et al*. [10] use the extended Kalman filter (EKF) to estimate the temperature and the state of charge of supercapacitors. El Mejdoubi *et al*. [11] develop an online supercapacitor's diagnosis model based on the EKF. This model has been validated experimentally using a noisy current profile and different aging phases. Using a Lyapunov-based adaptation law to estimate the supercapacitor's parameters, Chaoui *et al*. [12] proposed an online system identification method for lifetime diagnostic of supercapacitors. Moreover, Soualhi *et al.* [13] present a supercapacitor aging prediction method using artificial neural networks.

Manuscript received August 27, 2016; revised December 3, 2016; accepted January 9, 2017. Date of publication January 19, 2017; date of current version August 2, 2017. Recommended for publication by Associate Editor T. M. Lebey.

A. El Mejdoubi and H. Gualous are with the Laboratoire Universitaire des Sciences Appliquées de Cherbourg, Université de Caen Normandie, Cherbourg-Octeville 50130, France (e-mail: asmae.elmejdoubi@gmail.com; hamid.gualous@unicaen.fr).

H. Chaoui is with the Intelligent Robotic and Energy Systems research group, Department of Electronics, Carleton University, Ottawa, ON K1S 5B6, Canada (e-mail: hicham.chaoui@carleton.ca).

J. Sabor is with the Ecole Nationale Supérieure des Arts et Métiers, University Moulay Ismael, Meknes, 50050, Morocco (e-mail: sabor.jalal@hotmail.fr).

Color versions of one or more of the figures in this paper are available online at http://ieeexplore.ieee.org.

Digital Object Identifier 10.1109/TPEL.2017.2655578

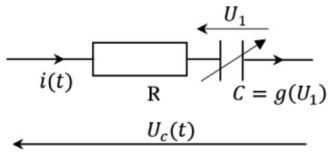


Fig. 1. Supercapacitor-*RC* circuit model.

The contribution of this paper is to propose an online SoH diagnosis model for supercapacitors using a sliding mode observer with an adaptation gain. The supercapacitor's model is considered as a nonlinear noisy system, which takes into account the variation of the capacitance as a function of the bias voltage, making the model highly nonlinear. While this increases complexity, it provides a more accurate representation of the system's dynamic. Sliding mode observers represent a class of very robust observers to parametric and modeling uncertainties. Such observers are based on the theory of variable structure systems which has several advantages such as rejecting external disturbances [14]. There exists a variety of sliding surfaces and appropriate selection is not trivial since this technique can be extended to higher order surfaces as the system's dimension increases. Many variations exist to limit the reluctance effect and optimize observation paths to raise the theoretical difficulties related to the discontinuities of observation [15]–[17]. In this paper, the proposed diagnosis model uses the adaptation of the sliding mode observer's gain at each calculation iteration to secure a minimum of the output observation error. A method to choose the design parameters has been developed so that the performance of a sliding-mode observer may be optimized for nonlinear noisy systems such as the system in hand. The effectiveness of the proposed method is verified by experimental results and compared against EIS. The rest of the paper is organized as follows: Section II outlines the circuit model of EDLCs. The proposed online diagnosis method is detailed in Section III. In Section IV, experimental results are reported, analyzed and compared. Finally, Section V presents conclusion with some remarks.

## II. EDLC Modeling

### A. EDLC Electric Modeling

The aim of our study is the online estimation of EDLCs aging indicators, namely the resistance and the capacitance, using the charging/discharging current and the bias voltage. Depending on the required accuracy and application, different electrical models have been developed so far for supercapacitors, and few models result in drastic increase in the system's nonlinear complexity [18]–[20]. Among those models, the *RC*-equivalent circuit, which is a lumped first-order transmission line model, is an effective model to represent the EDLC's dynamics, making it suitable for diagnosis purposes [21], [22].

In this electrical model, the EDLC, as presented in Fig. 1, is modeled by a capacitance *C* that can store and release electrical energy during charging and discharging cycles. This capacitance is composed by a constant part $C_0$ and a linear voltage dependent one $\alpha \cdot U_1$ where $\alpha$ is a coefficient which depends on the type of supercapacitor. Therefore, the current and the energy for a given voltage are higher than in the case of the classical expressions where the capacitance is constant [19]. As in any electrochemical process, these charging/discharging cycles encounter a small resistance due to the electrolyte and the interphase resistance. This small resistance (*R* in Fig. 1) appears in series with the EDLC capacitance. It is important to note that although such a model results in a drastic increase in the system's nonlinear complexity, it has been proved experimentally to provide a more accurate representation of the system's dynamics and a suitable model for both energy and electrical behaviors of EDLCs [23].

Therefore, the voltage–current characteristic dynamic model can be described by the following equations:

$$\begin{cases} U_c = U_1 + R \cdot i(t) \\ U_1 = \dfrac{1}{C} \cdot \int i(t)dt \end{cases} \tag{1}$$

where $U_c(t)$ and $i(t)$ are the supercapacitor voltage and its charge/discharge current, respectively. And the capacitance *C* is defined by the following relationship [19]:

$$C = g\left(U_1\right) = C_0 + \alpha \cdot U_1. \tag{2}$$

### B. State-Space Equations for the Model

The EDLCs' aging is the result of many degradation phenomena, which deteriorate the component performance over time until the end-of-life (EoL). This performance degradation is manifested by the resistance increase $R$ and the capacitance decrease $C$, so they are directly correlated to EDLCs' SoH. In this work, we assume that the system's parameters, i.e., $R$ and $C$, are assumed to be *a priori* unknown and the charging/discharging current $i(t)$ and the bias voltage $U_c$ are the only two values that are accessible from outside of system. We assumed also that the resistance is a slowly time-varying parameter such that $dR/dt = 0$ during a charge/discharge cycle. Also, the capacitance/voltage relationship evolves linearly with a constant or a slow time-varying slope $\alpha$ such that $d\alpha/dt = 0$.

Taking the derivative of (1) and (2) yields

$$\begin{cases} \dfrac{dU_1}{dt} = \dfrac{1}{C} \cdot i(t) + \dfrac{d}{dt}\left(\dfrac{1}{C}\right) \cdot \int i(t)dt \\ \dfrac{dC}{dt} = \alpha \cdot \dfrac{dU_1}{dt}. \end{cases} \tag{3}$$

Substituting for $dC/dt$ leads to

$$\begin{aligned} \frac{d}{dt}\left(\frac{1}{C}\right) &= -\frac{1}{C^2} \cdot \frac{dC}{dt} \\ &= -\frac{\alpha}{C^2} \cdot \left[\frac{1}{C} \cdot i(t) + \frac{d}{dt}\left(\frac{1}{C}\right) \cdot \int i(t)dt\right]. \end{aligned} \tag{4}$$

From the above-mentioned equations, the state vector X is chosen as follows:

$$\begin{cases} X = \begin{bmatrix} x_1 & x_2 & x_3 & x_4 \end{bmatrix}^T = \begin{bmatrix} U_1 & R & \dfrac{1}{C} & \alpha \end{bmatrix}^T \\ \dfrac{dX}{dt} = \begin{bmatrix} \dfrac{dx_1}{dt} & \dfrac{dx_2}{dt} & \dfrac{dx_3}{dt} & \dfrac{dx_4}{dt} \end{bmatrix}^T = \begin{bmatrix} \dfrac{dU_1}{dt} & \dfrac{dR}{dt} & \dfrac{d}{dt}\left(\dfrac{1}{C}\right) & \dfrac{d\alpha}{dt} \end{bmatrix}^T \end{cases}. \tag{5}$$

Based on the above-mentioned equations

$$\frac{dX}{dt} = \begin{pmatrix} 0 & 0 & i(t) & 0 \\ 0 & 0 & 0 & 0 \\ 0 & 0 & 0 & -{x_3}^3 \cdot .i(t) \\ 0 & 0 & 0 & 0 \end{pmatrix} \cdot X + \begin{pmatrix} 0 & 0 & \int i(t) & 0 \\ 0 & 0 & 0 & 0 \\ 0 & 0 & -{x_3}^2 \cdot .x_4 \cdot . \int i(t) & 0 \\ 0 & 0 & 0 & 0 \end{pmatrix} \cdot . \frac{dX}{dt}. \tag{6}$$

So

$$\frac{dX}{dt} = \begin{pmatrix} 0 & 0 & j & m \\ 0 & 0 & 0 & 0 \\ 0 & 0 & 0 & l \\ 0 & 0 & 0 & 0 \end{pmatrix} \cdot X = A \cdot X \tag{7}$$

with $j = \frac{i(t)}{1+x_4 \cdot {x_3}^2 \cdot \int idt}$, $l = \frac{-{x_3}^3 \cdot i(t)}{1+{x_3}^2 \cdot x_4 \cdot \int idt}$, and $m = \frac{-{x_3}^3 \cdot i(t) \cdot \int idt}{1+{x_3}^2 \cdot x_4 \cdot \int idt}$.

Indeed, the proposed diagnosis model will be used to estimate the state variables of a continuous nonlinear system with an external random noise defined by the system ($\Sigma$) defined as

$$(\Sigma) \begin{cases} \dot{X}(t) = A \cdot X + w(t) \\ Y(t) = U_c(t) = D \cdot X + v(t) \end{cases} \tag{8}$$

where $X$ is the state vector, $i(t)$ is the current as the input vector, $w(t)$ is the system disturbance vector, $U_c(t)$ is the bias voltage as the measurement vector, $v(t)$ is the channel noise, and $D = [\,1\ i(t)\ \ 0\ 0\,]$.

The vectors $w(t)$ and $v(t)$ are Gaussian white noises with unknown statistics: the only information of these disturbances concerns their norm upper bounds $W > 0$ and $V > 0$ such that $w(t) < W$ and $v(t) < V$.

### C. Observability of the State Model

Before elaborating the diagnosis model, it must first ensure that the state model is observable. As we are in the case of a nonlinear system, we study the system observability around its equilibrium point $X = X_{\text{eq}}$ using the Jacobian matrix [24].

Considering *n* as the system order, the Jacobian matrix of the system is defined by [24]

$$J(X_{\text{eq}}) = \frac{\partial}{\partial X} \begin{bmatrix} h(X,i) \\ (L_f h)(X,i) \\ \vdots \\ (L_f^{n-1} h)(X,i) \end{bmatrix} \Bigg|_{X = X_{\text{eq}}}. \tag{9}$$

And $L_f$ is an operator calculated as follows [25]:

$$(L_f h)(X,i) = \left[\frac{\partial h(X,i)}{\partial X}\right] f(X,i) + \left[\frac{\partial h(X,i)}{\partial i}\right] \frac{di}{dt}. \tag{10}$$

Thus, the matrix is given by

$$J(X_{\text{eq}}) = \begin{bmatrix} 1 & i(t) & 0 & 0 \\ 0 & \dfrac{di}{dt} & j & m \\ 0 & \dfrac{d^2 i}{dt^2} & \dfrac{\partial j}{\partial X} & \dfrac{\partial m}{\partial X} \\ 0 & \dfrac{d^3 i}{dt^3} & \dfrac{\partial^2 j}{\partial X^2} & \dfrac{\partial^2 m}{\partial X^2} \end{bmatrix}. \tag{11}$$

We note that $rang(J(X_{\text{eq}})) = 4 = system\ order$.

Therefore, the system is observable around its equilibrium point $X_{\text{eq}}$.

## III. Diagnosis Model

### A. Sliding Mode Observer for EDLC Diagnosis

The application of the sliding mode observer to the diagnostic of supercapacitor is original and has some fundamentally numerous advantages [17], [26]. The sliding surface attractiveness is provided by condition called sliding conditions. If these conditions are verified, the system converges to the sliding surface and there changes according to a fixed velocity. We note that in the case of sliding modes observers, the estimation errors $\tilde{X}(t) = X(t) - \hat{X}(t)$ are considered important for the dynamic observation sliding modes [26].

The convergence of the estimation errors to equilibrium values is ensured in two steps [27]:

1) *Reaching phase:* estimation errors follow a trajectory to reach the sliding surface where the estimation error is zero.
2) *Sliding phase:* the estimation errors slide on the sliding surface to cancel the observation error with the correction gain that acts to satisfy the following invariance conditions: $S = 0$ and $\dot{S} = 0$. We note that the stability should be checked to assess the quality of convergence and stability of the proposed model.

A nonlinear sliding mode observer is proposed whose structure is the following:

$$\dot{\hat{X}} = A_s \cdot \hat{X} + L \cdot \left(Y - D \cdot \hat{X}\right) + S \tag{12}$$

where $A_s$ is the sliding mode observer matrix, $S$ is the sliding surface, and $L$ is the adaptation gain.

Whether $\hat{X}_0$ is the initial state of estimated state vector X and $\tilde{X}(t) = X(t) - \hat{X}(t)$ the estimation error of the state vector.

Based on (8) and (12), the estimation error is

$$\begin{aligned} \dot{\tilde{X}} &= \dot{X} - \dot{\hat{X}} = AX + w - \left(A_g \hat{X} + L\left[DX - D\tilde{X}\right] + S\right) \\ &= (A - LD) \cdot \tilde{X} + (A - A_s) \cdot \hat{X} - S + w. \end{aligned} \tag{13}$$

As the noises $w$ and $v$ are Gaussian white noises and the system variables are random variables, then the estimation error

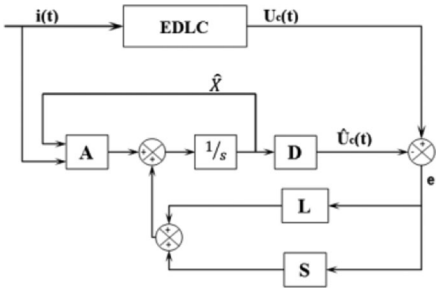


Fig. 2. Functional diagram of sliding mode observer.

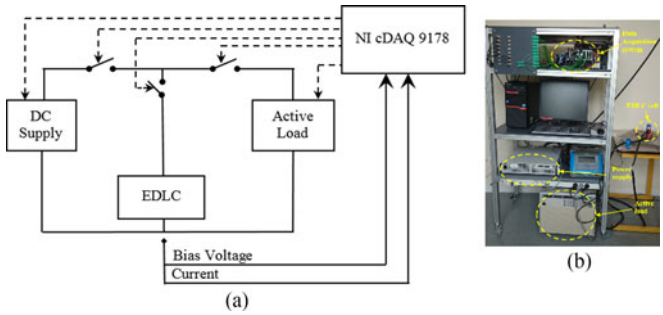


Fig. 3. Test bench used for characterization: (a) Illustration of the test bench and (b) test bench.

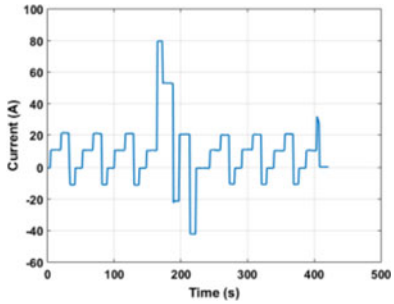


Fig. 4. Applied current profile.

$\tilde{X}$ is a Gaussian random variable. So expectancy $\tilde{X}$ tends to 0 if and only if the proposed observer in (9) is unbiased [28]

$$\mathrm{E}\left[\dot{\hat{X}}(t)\right] = (A - L \cdot D) \cdot E\left[\tilde{X}\right] + (A - A_s) \cdot E[\hat{X}]. \quad (14)$$

Then, the observer is unbiased if and if only the following conditions are verified [28]:

$$\begin{cases} A_s = A \\ A - L \cdot D \text{ is stable} \end{cases}. \quad (15)$$

So, replacing $A_s$ by the obtained equation (15) in (12), we obtain

$$\dot{\hat{X}} = A \cdot \hat{X} + L \cdot \left(Y - D \cdot \hat{X}\right) + S. \quad (16)$$

Thus, the structure of the proposed sliding mode observer can be represented by Fig. 2.

The adaptation gain can be expressed as (details in Appendix I)

$$L = P \cdot D^T \cdot \left(V + D \cdot P \cdot D^T\right)^{-1} \quad (17)$$

where

$$P(t + dt) = (I + A \cdot dt) \cdot P(t) \cdot (I + A \cdot dt)^T + W \cdot dt. \quad (18)$$

*Theorem 1:* The convergence of the system is ensured to the sliding surface *S* defined by

$$S = \begin{cases} \dfrac{P^{-1} \cdot D^T \cdot \left(Y - D \cdot \hat{X}\right)}{Y - D \cdot \hat{X}} \text{ if } Y - D \cdot \hat{X} > \varepsilon \\ \dfrac{P^{-1} \cdot D^T \cdot \left(Y - D \cdot \hat{X}\right)}{\varepsilon} \text{ if } Y - D \cdot \hat{X} \leq \varepsilon \end{cases} \quad (19)$$

where $\varepsilon$ is the amplitude of the boundary layer of the bias voltage estimated error.

Proof 1 is presented in Appendix II

if $Y - D \cdot \hat{X} = \tilde{Y} > \varepsilon$, the system is stable in the sense of Lyapunov if $\exists a_1 > 0$ and $b_1 > 0$ verify $\tilde{X} > \frac{-b_1}{a_1}$.

if $Y - D \cdot \hat{X} = \tilde{Y} \leq \varepsilon$, the system is stable in the sense of Lyapunov.

## IV. Experimental Results

### A. Characterization Test Bench

In this experimental setup, the supercapacitors are charged and discharged under a current profile at chosen constant temperature, where the bias voltage and the charge/discharge current are measured and saved using the acquisition board NI cDAQ 9178 and LabView software as presented in Fig. 3. Then, the supercapacitors undergo a calendar aging. The supercapacitors calendar aging is already presented in the literature where the supercapacitors are placed inside the climatic chamber and are connected to the voltage sources for few days [11], [29]. Finally, the supercapacitors are taken out of the climatic chamber to be characterized using the same conditions of temperature and current profile. This process is repeated until the limit of aging is reached.

The EDLC discharge phase has been done at a standardized dynamic current profile as presented in Fig. 4, which represents the supercapacitor behavior in vehicular applications compared to the current profiles already presented in the existing works [30]. Thus, this current profile presents the acceleration and the braking conditions, which reflects the real driving profile in electrical vehicle applications.

### B. Nominal Results

In this study, two 1500F supercapacitors BCAP1500 de Maxwell Technologies are used for tests. They are placed inside a temperature-controlled chamber, in which temperature is set to 65 °C with a continuous applied voltage of 2.7 V. Five milestones are set for the aging process, i.e., 0 (brand new), 141,

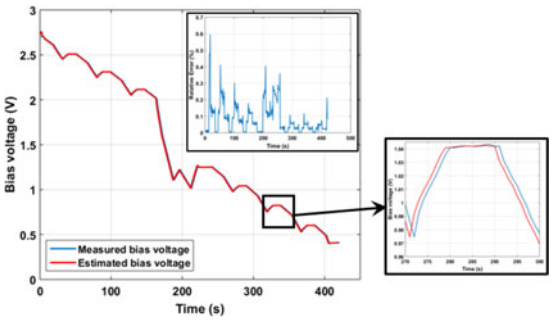


Fig. 5. Estimation of the bias voltage using the sliding mode observer.

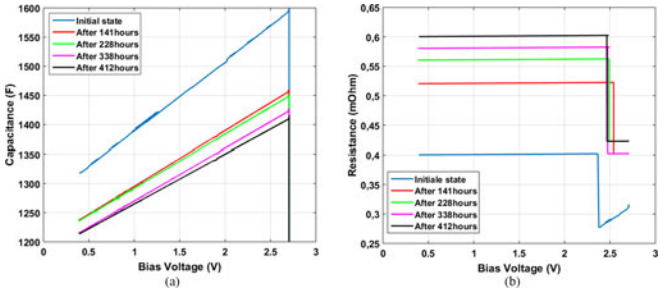


Fig. 6. Estimation of the supercapacitor's parameters using the sliding mode observer, (a) capacitance and (b) resistance.

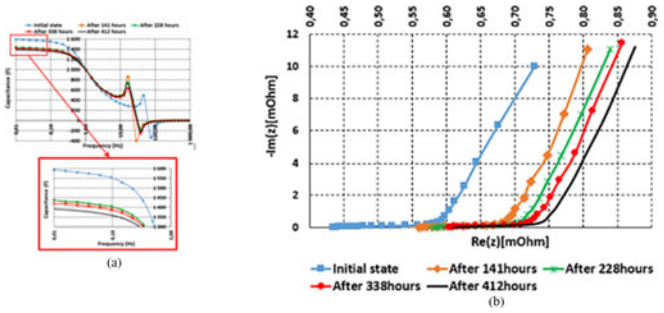


Fig. 7. EDLC parameters frequency behavior, (a) capacitance and (b) resistance.

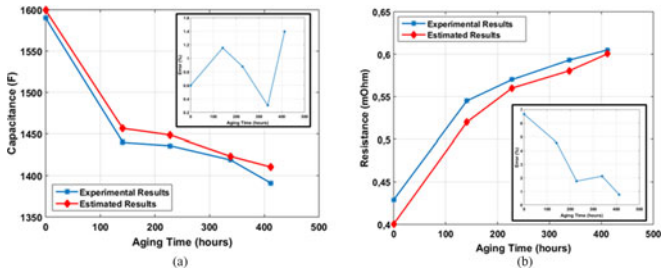


Fig. 8. Comparison between the estimated and EIS results, (a) capacitance and (b) resistance.

228, 338, and 412 h (EoL). The data measurements' sampling time is set to 0.01 s.

*1) Bias Voltage Observation:* Fig. 5 presents a comparison between the measured and the estimated bias voltage using the proposed sliding mode observer.

We note that the transitional phase of the bias voltage observation is negligible. In addition, a perfect tracking is achieved and the average relative error remains very small as presented in Fig. 5 during all experiments. The high accuracy of the proposed observer is clearly shown in this experiment.

We note that the relative error decreases with the estimation and observation evolution using the sliding mode observer. The sliding mode observation is an extension of sliding mode control in the state estimation by an observer. Using the same theory as sliding mode control, the sliding mode observation trajectories are constrained to evolve in finite time on a suitable sliding manifold by the use of a discontinuous switching law. Constrained to the suitable sliding manifold, the resultant states are shown to be insensitive to uncertainty and random disturbance [31], [32].

*2) Sliding Mode Observer Diagnosis Results:* An experiment is conducted using the aforementioned current profile. Results of the diagnosis using the sliding mode observer are depicted in Fig. 6. As it is revealed, both resistance and capacitance estimates show good convergence despite of current's profile nonlinearities.

In addition, the evolutions of the estimated resistance and capacitance follow their theoretical evolution, where for the same bias voltage, the capacitance decreases and the resistance increases with the increase of the aging time.

*3) Impedance Spectroscopy Characterization:* The impedance spectroscopy characterization provides a powerful tool of analysis and investigation of supercapacitor dynamics behavior according to dynamic constraints. It consists to excite the EDLC under test with small alternative current and to measure the bias voltage, where the impedance amplitude is calculated as a ratio between the alternative voltage amplitude and the alternative current amplitude, and the impedance phase is calculated as a difference between alternative signals arguments.

The impedance spectroscopy measurements are realized with Zahner ZENNIUM+PP241 impedance analyzers. THALES software ensured the data acquisition and the control function with good quality by varying the frequency of the alternative ac current from 10 mHz to 100 kHz for a supercapacitor charged at 2.7 V.

Fig. 7 presents the resistance and the capacitance frequency behavior of the supercapacitor for the five aging phases. We notice that some errors appear in low impedance supercapacitors at high frequencies. They are caused by the coupling effects between current feeding and potential sensing lines and diminish at low frequencies but become dramatic at high frequencies [1], [33].

In order to validate the estimated parameters using the sliding mode observer, a comparison between the estimated parameters and EIS's results is presented in Fig. 8, where the parameters have been calculated using the following equations:

$$\begin{cases} \text{Experimental resistance} = R_b = R_{\text{EIS}}\left(-\text{Im}_{\max}(z)\right) \\ \text{Estimated resistance} = \lim\limits_{U_c=0.5\text{V}} R_{\text{estimated}} \\ \text{Experimental capacitance} = C_{\text{EIS}}\ \ (0.01\ \text{Hz}) \\ \text{Estimated capacitance}\ = C_{\text{estimated}}\ \ (\ U_c = 2.7\ \text{V}\ ). \end{cases} \tag{20}$$

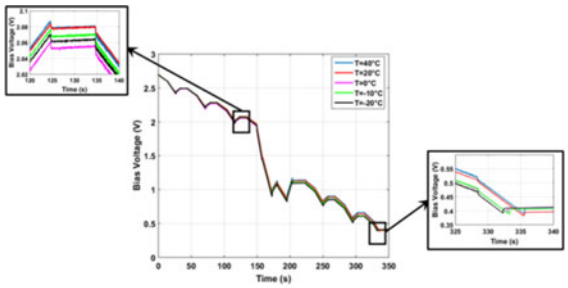


Fig. 9. Bias voltage evolution of supercapacitors characterized under different temperatures.

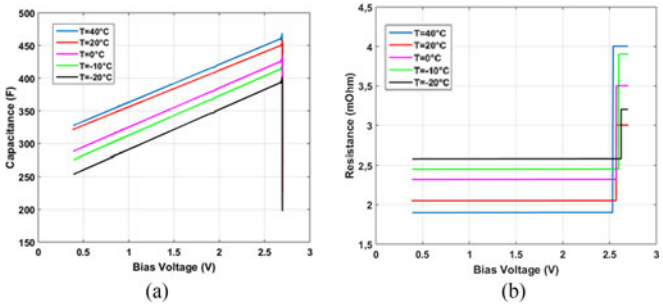


Fig. 10. Estimation of the supercapacitor's parameters using the sliding mode observer for different temperature characterizations, (a) capacitance and (b) resistance.

The obtained estimated results confirm the theoretical evolution. The capacitance evolution decreases and the resistance evolution increases with the aging time. Indeed, the comparison of measured and estimated efficiency values shows that these values are nearly identical. The difference between the experimental and the estimated results is clearly small. Nevertheless, the error never exceeds 1.4% for the capacitance estimation and 6.8% for the resistance estimation, as presented in Fig. 8. As the threshold of the capacitance EoL corresponds to 80% from the initial capacitance value, a maximum estimation error of 1.4% is very acceptable. Also, compared to 200% from the initial resistance as the resistance EoL threshold, 6.8% as a maximum estimation error is very admissible.

### C. Temperature Validation

In order to study the effect of temperature on the aging indicators, two supercapacitors 310F (BCAP0310) from Maxwell Technologies at different aging conditions are characterized using the current profile in Fig. 4. Fig. 9 presents the observed bias voltage using the proposed sliding mode observer for new supercapacitors characterized under different temperatures conditions (–20 °C, –10 °C, 0 °C, 20 °C, and 40 °C) and a constant applied bias voltage (2.7 V).

We notice that, for the same discharge time, the bias voltage increases with the increase in temperature, this increase in bias voltage results from the decrease in resistance. Also, the discharge full time, representing the full EDLC capacitance, increases with the increase in temperature.

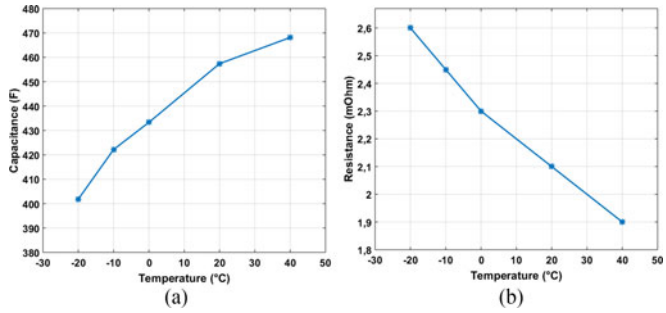


Fig. 11. EDLC's parameters evolution with the temperature characterization, (a) capacitance and (b) resistance.

Using the proposed sliding mode observer, Fig. 10 presents the EDLC's parameters evolution for different temperature characterizations.

In Fig. 11, we can see that the resistance value at the same aging phase is decreased by increasing temperature. It should be mentioned that the electrolyte assures a link between the two electrodes: the cathode and the anode, presented in the electric model by the resistance. So, the resistance evolution is an image of the electrolyte parameters such as the viscosity and the reaction speed. The increase in resistance as the operating temperature decreases is due to the increase of the electrolyte's viscosity which generates the decrease in redox reaction speed [1], [7].

In addition, it can be seen that the capacitance decreases when the temperature decreases. We thus conclude that the supercapacitor global capacitance slightly increases with the increase in temperature, as confirmed by Fig. 11(b). The consequence of the decrease of the supercapacitor capacitance with temperature is that energy storage in the supercapacitor is lower for low temperature values [1].

In vehicular applications, high performance needs to be achieved without added computational burden since the onboard computation power is limited. To evaluate this aspect, a comparison between the characteristics of the proposed diagnosis model and the EKF is presented in [11]. The proposed method yields 12 computational operations as opposed to 14 for EKF. The reduced operations result in more than 20% decrease in computational burden (112 $\mu$s vs. 126 $\mu$s), which is significant for online applications such as electric vehicles. Therefore, the proposed sliding mode observer based diagnostic method is more efficient in estimating the EDLCs aging indicators.

## V. Conclusion

In this paper, an online aging diagnosis method is presented for supercapacitors. The proposed strategy capitalizes on the capabilities of the nonlinear sliding mode observer to estimate the EDLCs parameters. Therefore, online parameter estimation is achieved, which yields to SoH prediction. The effectiveness of this observer is presented through a series of experiments using a standardized dynamic current profile that reflects the real driving profile in electrical vehicle applications. The results highlight the good performance of the proposed diagnosis

model. Comparison of the estimated capacitance and resistance against EIS shows acceptable errors compared to the indicators thresholds, and proves the high quality of the proposed observer to estimate the EDLCs aging indicators, which yields to accurate SoH prediction.

## APPENDIX I

To achieve the best estimate of state vector $X$, it is necessary that the estimation error variance is minimal. Thus, the estimation error variance verifies the following quadratic cost functional [34]:

$$J(t) = \sum E\left[\tilde{X}_i^2(t)\right] = E\left[\tilde{X}^T(t)\cdot\tilde{X}(t)\right] = \operatorname{tr}\left(E\left[\tilde{X}(t)\cdot\tilde{X}^T(t)\right]\right). \tag{AI.1}$$

By substituting the covariance matrix of the estimation error $P(t)$ which satisfies the following equation [35]:

$$P(t) = E\left[\tilde{X}(t)\cdot\tilde{X}^T(t)\right]. \tag{AI.2}$$

According to (AI. 2), $P(t)$ is given by the mathematical expectation of the random variable $\tilde{X}(t)\cdot\tilde{X}^T(t)$. Thus, based on the definition of the mathematical expectation of a random variable, we have [34], [36]

$$P(t) = \int\left[\left(\tilde{X}(t)\cdot\tilde{X}^T(t)\right)\cdot A\left(\tilde{X}(t)\cdot\tilde{X}^T(t)\right)\right]dX. \tag{AI.3}$$

The development of (AI. 3) by replacing the vector $\tilde{X}(t)$ by its own value such as [34], [36]

$$\dot{P}(t) = (A - L\cdot D)\cdot P(t) + P(t)\cdot(A - L\cdot D)^T + L\cdot V\cdot L^T + W. \tag{AI.4}$$

To minimize the trace of $P(t)$ compared to $L$ at each time $t$, simply minimize $\operatorname{tr}(\dot{P}(t))$ [37]

$$\frac{\partial\left(\operatorname{trace}\dot{P}(t)\right)}{\partial K} = -P(t)\cdot D^T - P(t)\cdot D^T + 2\cdot L\cdot V. \tag{AI.5}$$

So

$$L = P\cdot D^T\cdot V^{-1}. \tag{AI.6}$$

Thus, (AI. 4) becomes

$$\dot{P}(t) = A\cdot P(t) + P(t)\cdot A^T - P(t)\cdot D^T\cdot V^{-1}\cdot D\cdot P(t) + W. \tag{AI.7}$$

This Riccati differential equation must be integrated and initialized with $P(t_0)$, which presents the confidence that we have in the observer initialization with $\hat{X}_0(t)$.

At time *t*, the estimation error is characterized by $P(t)$. The solution of the differential equation Riccati presented in (AI. 7) shows that the error can only increase and the prediction error at $(t + dt)$ is characterized by

$$P(t+dt) = (I + A\cdot dt)\cdot P(t)\cdot(I + A\cdot dt)^T + W\cdot dt. \tag{AI.8}$$

The sliding mode observer gain $L$ is calculated based on the covariance matrix of the estimation error $P(t)$. Using this gain, the estimated state vector $\hat{X}$ and the covariance matrix of the estimation error $P$ are readjusted at time $(t + dt)$ based on the results obtained in the estimation of the previous iteration step $t$

$$\hat{X}(t+dt) = P(t) + L\cdot(Y - D\cdot P(t)). \tag{AI.9}$$

Using the model equation, we can write

$$X(t+dt) - \hat{X}(t+dt) = (I - L\cdot D)\left(X(t) - \hat{X}(t) - L\cdot V\cdot L^T\right). \tag{AI.10}$$

So

$$P(t+dt) = (I - L\cdot D)\cdot P(t)\cdot(I - L\cdot D)^T + L\cdot V\cdot L^T. \tag{AI.11}$$

And

$$(A - LD)^T P + P(A - LD) - P\cdot V^{-1}\cdot P + W = \dot{P} = -Q < 0 \tag{AI.12}$$

where *Q* is a positive definite matrix.

We can deduce

$$L = P\cdot D^T\cdot\left(V + D\cdot P\cdot D^T\right)^{-1}. \tag{AI.13}$$

## APPENDIX II

*Theorem 1:* The convergence of the system is ensured to the sliding surface S defined by

$$S = \begin{cases} \dfrac{P^{-1}\cdot D^T\cdot\left(Y - D\cdot\hat{X}\right)}{\|Y - D\cdot\hat{X}\|} & \text{if} \|Y - D\cdot\hat{X}\| > \varepsilon \\ \dfrac{P^{-1}\cdot D^T\cdot\left(Y - D\cdot\hat{X}\right)}{\varepsilon} & \text{if } \|Y - D\cdot\hat{X}\| \le \varepsilon \end{cases} \tag{AII.1}$$

where $\varepsilon$ is the amplitude of the boundary layer of the bias voltage estimated error.

*Proof 1:* Choose the following Lyapunov candidate:

$$V = \tilde{X}^T\cdot P\cdot\tilde{X} \tag{AII.2}$$

where $X = X - \hat{X}$.

Taking the derivative the Lyapunov function leads to

$$\dot{V} = 2\cdot\tilde{X}^T\cdot P\cdot\dot{\tilde{X}} \tag{AII.3}$$

Such as

$$\dot{\tilde{X}} = X - \dot{\hat{X}} = AX - \left(A\hat{X} + L\tilde{Y} + S\right) = A\tilde{X} - L\tilde{Y} - S \tag{AII.4}$$

where $\tilde{Y} = Y - \hat{Y}$.

Adding and subtracting $LD\tilde{X}$

$$\dot{\tilde{X}} = (A - LD)\,\tilde{X} - L\left(\tilde{Y} - D\tilde{X}\right) - S. \tag{AII.5}$$

However

$$\tilde{Y} = Y - \hat{Y} = DX - D\hat{X} = D\tilde{X}. \tag{AII.6}$$

So, $\tilde{Y} - D\tilde{X} = 0$

$$\dot{\tilde{X}} = (A - LD)\,\tilde{X} - S. \tag{AII.7}$$

Substituting for $\dot{\tilde{X}}$ yields

$$\begin{aligned}\dot{V} &= 2 \cdot \tilde{X}^T \cdot P \cdot \left[(A - LD)\,\tilde{X} - S\right] \\ &= \tilde{X}^T \cdot [2P\,(A - LD)]\,\tilde{X} - 2\tilde{X}^T \cdot P \cdot S \\ \dot{V} &= -\tilde{X}^T \cdot Q \cdot \tilde{X} - 2\tilde{X}^T \cdot P \cdot S. \end{aligned} \tag{AII.8}$$

Two cases have to been considered: $\|Y - D \cdot \hat{X}\| > \varepsilon$ (Case 1) and $\|Y - D \cdot \hat{X}\| \leq \varepsilon$ (Case 2).

*Case 1:* if $\|Y - D \cdot \hat{X}\| = \|\tilde{Y}\| > \varepsilon$

$$\dot{V} = -\tilde{X}^T \cdot Q \cdot \tilde{X} - \frac{2\tilde{X}^T \cdot D^T \cdot \tilde{Y}}{\|\tilde{Y}\|}. \tag{AII.9}$$

Or, we have

$$\|\tilde{Y}\| = \|D\tilde{X}\| \leq \|D\| \cdot \|\tilde{X}\|. \tag{AII.10}$$

So

$$\dot{V} \leq -\tilde{X}^T \cdot Q \cdot \tilde{X} - \frac{2\tilde{X}^T \cdot D^T \cdot D \cdot \tilde{X}}{\|D\|\|\tilde{X}\|} \tag{AII.11}$$

where $\exists(a_1, b_1) \in \Re^2$, $\dot{V} \leq -a_1 \cdot \|\tilde{X}\|^2 - b_1 \cdot \|\tilde{X}\|$.

Thus, $\dot{V} \leq 0$, if $\|\tilde{X}\| > \frac{-b_1}{a_1}$.

Choosing $a_1 > 0$ and $b_1 > 0$ so that $\dot{V} \leq 0$ guarantees the system's stability to a neighborhood of $\tilde{X} = 0$. Therefore, the system is stable in the sense of Lyapunov in the case of $\|Y - D \cdot \hat{X}\| = \|\tilde{Y}\| > \varepsilon$.

*Case 2:* if $\|Y - D \cdot \hat{X}\| = \|\tilde{Y}\| \leq \varepsilon$

$$\begin{aligned}\dot{V} &= -\tilde{X}^T \cdot Q \cdot \tilde{X} - \frac{2\tilde{X}^T \cdot D^T \cdot \tilde{Y}}{\varepsilon} \\ &= -\tilde{X}^T \cdot Q \cdot \tilde{X} - \frac{2\tilde{X}^T \cdot D^T \cdot D \cdot \tilde{X}}{\varepsilon}. \end{aligned} \tag{AII.12}$$

So

$$\dot{V} = -\tilde{X}^T \cdot \left[Q + \frac{2 \cdot D^T \cdot D}{\varepsilon}\right] \cdot \tilde{X} \leq -\left[Q + \frac{2 \cdot D^2}{\varepsilon}\right] \cdot \|\tilde{X}^2\| \tag{AII.13}$$

where $[Q + \frac{2 \cdot \|D\|^2}{\varepsilon}] \cdot \|\tilde{X}^2\| \geq 0$.

Thus, $\dot{V} \leq 0$.

Therefore, the system is stable in the sense of Lyapunov in the case of $\|Y - D \cdot \hat{X}\| = \|\tilde{Y}\| \leq \varepsilon$.

*Conclusion:* If $\|Y - D \cdot \hat{X}\| = \|\tilde{Y}\| > \varepsilon$, the system is stable in the sense of Lyapunov if $\exists a_1 > 0$ and $b_1 > 0$ verify $\|\tilde{X}\| > \frac{-b_1}{a_1}$.

if $\|Y - D \cdot \hat{X}\| = \|\tilde{Y}\| \leq \varepsilon$, the system is stable in the sense of Lyapunov.

## REFERENCES


[1] H. Gualous, H. Louahlia, and R. Gallay, "Supercapacitor characterization and thermal modelling with reversible and irreversible heat effect," *IEEE Trans. Power Electron.*, vol. 26, no. 11, pp. 3402–3409, Nov. 2011.

[2] A. Allagui, A. S. Elwakil, B. J. Maundy, and T. J. Freeborn, "Spectral capacitance of series and parallel combinations of supercapacitors," *ChemElectroChem*, vol. 3, pp. 1429–1436, 2016.

[3] A. Kuperman *et al.*, "Supercapacitor sizing based on desired power and energy performance," *IEEE Trans. Power Electron.*, vol. 29, no. 10, pp. 5399–5405, Oct. 2014.

[4] R. German, A. Hammar, R. Lallemand, A. Sari, and P. Venet, "Novel experimental identification method for a supercapacitor multipore model in order to monitor the state of health," *IEEE Trans. Power Electron.*, vol. 31, no. 1, pp. 548–559, Jan. 2016.

[5] Y. Diab, P. Venet, H. Gualous, and G. Rojat, "Self-discharge characterization and modeling of electrochemical capacitor used for power electronics applications," *IEEE Trans. Power Electron.*, vol. 24, no. 2, pp. 510–517, Feb. 2009.

[6] D. Iannuzzi and P. Tricoli, "Speed-based state-of-charge tracking control for metro trains with onboard supercapacitors," *IEEE Trans. Power Electron.*, vol. 27, no. 4, pp. 2129–2140, Apr. 2012.

[7] A. Hammar, P. Venet, R. Lallemand, G. Coquery, and G. Rojat, "Study of accelerated aging of supercapacitors for transport applications," *IEEE Trans. Ind. Electron.*, vol. 57, no. 12, pp. 3972–3979, Dec. 2010.

[8] M. Marracci, B. Tellini, M. Catelani, and L. Ciani, "Ultracapacitor degradation state diagnosis via electrochemical impedance spectroscopy," *IEEE Trans. Instrum. Meas.*, vol. 64, no. 7, pp. 1916–1921, Jul. 2015.

[9] A. Nadeau, G. Sharma, and T. Soyata, "State-of-charge estimation for supercapacitors: A Kalman filtering formulation," in *Proc. IEEE Int. Conf. Acoust., Speech Signal Process.*, Florence, Italy, 2014, pp. 2194–2198.

[10] C.-J. Chiang, J.-L. Yang, and W.-C. Cheng, "Temperature and state-of-charge estimation in ultracapacitors based on extended Kalman filter," *J. Power Sources*, vol. 234, pp. 234–243, 2013.

[11] A. El Mejdoubi, A. Oukaour, H. Chaoui, Y. Slamani, J. Sabor, and H. Gualous, "Online supercapacitor diagnosis for electric vehicle applications," *IEEE Trans. Veh. Technol.*, vol. 65, no. 6, pp. 4241–4252, Jun. 2016.

[12] H. Chaoui, A. El Mejdoubi, A. Oukaour, and H. Gualous, "Online system identification for lifetime diagnostic of supercapacitors with guaranteed stability," *IEEE Trans. Control Syst. Technol.*, vol. 24, no. 6, pp. 2094–2102, Nov. 2016.

[13] A. Soualhi *et al.*, "Supercapacitors ageing prediction by neural networks," in *Proc. 39th Annu. Conf. IEEE Ind. Electron. Soc.*, Vienna, Austria, 2013, pp. 6812–6818.

[14] I.-S. Kim, "A technique for estimating the state of health of lithium batteries through a dual-sliding-mode observer," *IEEE Trans. Power Electron.*, vol. 25, no. 4, pp. 1013–1022, Apr. 2010.

[15] X. Zhang, L. Sun, K. Zhao, and L. Sun, "Nonlinear speed control for PMSM system using sliding-mode control and disturbance compensation techniques," *IEEE Trans. Power Electron.*, vol. 28, no. 3, pp. 1358–1365, Mar. 2013.

[16] K. C. Veluvolu and Y. C. Soh, "High-gain observers with sliding mode for state and unknown input estimations," *IEEE Trans. Ind. Electron.*, vol. 56, no. 9, pp. 3386–3393, Jun. 2009.

[17] L. M. Capisani, A. Ferrara, A. F. d. Loza, and L. M. Fridman, "Manipulator fault diagnosis via higher order sliding-mode observers," *IEEE Trans. Ind. Electron.*, vol. 59, no. 10, pp. 3979–3986, Apr. 2012.

[18] S. Jayasinghe and D. Vilathgamuwa, "Flying supercapacitors as power smoothing elements in wind generation," *IEEE Trans. Ind. Electron.*, vol. 60, no. 7, pp. 2909–2918, Jul. 2013.

[19] L. Zubieta and R. Bonert, "Characterization of double-layer capacitors for power electronics applications," *IEEE Trans. Ind. Appl.*, vol. 36, no. 1, pp. 199–205, Jan./Feb. 2000.

[20] A. Hijazi, P. Kreczanik, E. Bideaux, P. Venet, G. Clerc and M. D. Loreto, "Thermal network model of supercapacitors stack," *IEEE Trans. Ind. Electron.*, vol. 59, no. 2, pp. 979–987, Feb. 2012.

[21] H. Liu, Z. Wang, J. Cheng, and D. Maly, "Improvement on the cold cranking capacity of commercial vehicle by using supercapacitor and lead-acid battery hybrid," *IEEE Trans. Veh. Technol.*, vol. 58, no. 3, pp. 1097–1105, Mar. 2009.

[22] N. Rizoug, P. Bartholomeus, and P. L. Moigne, "Study of the ageing process of a supercapacitor module using direct method of characterization," *IEEE Trans. Energy Convers.*, vol. 27, no. 2, pp. 220–228, Jun. 2012.

[23] N. Rizoug, P. Bartholomeus, and P. L. Moigne, "Modeling and characterizing supercapacitors using an online method," *IEEE Trans. Ind. Electron.*, vol. 57, no. 12, pp. 3980–3990, Dec. 2010.

[24] B. Gou, "Jacobian matrix-based observability analysis for state estimation," *IEEE Trans. Power Syst.*, vol. 21, no. 1, pp. 348–356, Feb. 2006.

[25] G. Rigatos, P. Siano, N. Zervos, and C. Cecati, "Control and disturbances compensation for doubly fed induction generators using the derivative-free nonlinear kalman filter," *IEEE Trans. Power Electron.*, vol. 30, no. 10, pp. 5532–5547, Oct. 2015.
[26] L. Fridman, Y. Shtessel, C. Edwards, and X.-G. Yan, "Higher-order sliding-mode observer for state estimation and input reconstruction in nonlinear systems," *Int. J. Robust Nonlinear Control*, vol. 18, pp. 399–412, 2007.
[27] Y. Xing-Gang and C. Edwards, "Robust sliding mode observer-based actuator fault detection and isolation for a class of nonlinear systems," in *Proc. 44th IEEE Conf. Decis. Control*, 2005, pp. 987–992.
[28] H. S. Ali, M. Alma, M. Darouach, and C. Delattre, "Design of unbiased functional observers for interconnected discrete-time delay systems," in *Proc. 3rd Int. Conf. Syst. Control*, 2013, pp. 534–539.
[29] A. El Mejdoubi, A. Oukaour, H. Chaoui, H. Gualous, J. Sabor, and Y. Slamani, "Prediction aging model for supercapacitor's calendar life in vehicular applications," *IEEE Trans. Veh. Technol.*, vol. 65, no. 6, pp. 4253–4263, Jun. 2016.
[30] Electric Double-Layer Capacitors for Use in Hybrid Electric Vehicles—Test Methods for Electrical Characteristics, IEC Std. 62576, 2009.
[31] S. Shao, P. W. Wheeler, J. C. Clare, and A. J. Watson, "Fault detection for modular multilevel converters based on sliding mode observer," *IEEE Trans. Power Electron.*, vol. 28, no. 11, pp. 4867–4872, Nov. 2013.
[32] X. Zhang and Z. Li, "Sliding-mode observer-based mechanical parameter estimation for permanent magnet synchronous motor" *IEEE Trans. Power Electron.*, vol. 31, no. 8, pp. 5732–5745, Aug. 2016.
[33] R. German, P. Venet, A. Sari, O. Briat, and J.-M. Vinassa, "Improved supercapacitor floating ageing interpretation through multipore impedance model parameters evolution," *IEEE Trans. Power Electron.*, vol. 29, no. 7, pp. 3669–3678, Jul. 2014.
[34] T. Nguyen and Z. Gajic, "Solving the matrix differential Riccati equation: A lyapunov equation approach," *IEEE Trans. Autom. Control*, vol. 55, no. 1, pp. 191–194, Jan. 2010.
[35] Z. Chen, Y. Fu, and C. Mi, "State of charge estimation of lithium-ion batteries in electric drive vehicles using extended kalman filtering," *IEEE Trans. Veh. Technol.*, vol. 62, no. 3, pp. 1020–1030, Mar. 2013.
[36] E. Kozhanova and A. Zaharov, "Application of wavelet analysis to determine the parameters of the normal distribution law," in *Proc. Int. Conf. Actual Probl. Electron Devices Eng.*, 2014, pp. 280–283.
[37] T. Stillfjord, "Low-rank second-order splitting of large-scale differential Riccati equations," *IEEE Trans. Autom. Control*, vol. 60, no. 10, pp. 2791–2796, Oct. 2015.

**Asmae El Mejdoubi** (S'15–M'16) was born in Morocco in 1988. She received the Engineering degree in electromechanical engineering from the Ecole Nationale Supérieure d'Arts & Métiers "ENSAM," Meknès, Morocco, in 2012, and the Ph.D. degree in electrical engineering jointly from the University of Caen Normandie, Caen, France, and the l'ENSAM de l'Université Moulay Ismaïl, Meknes, Morocco, in 2015.

She is a Postdoctoral Fellow in the Laboratoire Universitaire des Sciences Appliquées de Cherbourg Laboratory, Université de Caen Normandie. Her research interests include the area of energy storage, more specifically, supercapacitors and lithium-ion batteries, state-of-health and state-of-charge diagnosis, and aging estimation.

**Hicham Chaoui** (S'01–M'12–SM'13) received the B.Sc. degree in electrical engineering from the Institut superieur du Génie Appliqué, Casablanca, Morocco, in 1999, the M.A.Sc. degree in electrical engineering, the M.Sc. degree in computer science (with honors), the Graduate degree in project management, and the Ph.D. degree in electrical engineering (with honors) all from the University of Quebec, Montreal, QC, Canada, in 2003, 2005, 2007, and 2012, respectively.

His career has spanned both academia and industry in the field of intelligent control and renewable energies. Prior to his academic career, he held various engineering and management positions including the Vice-President of Innovation and Technology Development, TDE Techno Design, Montreal, QC, Canada. From 2014 to 2016, he had been an Assistant Professor with the Tennessee Technological University, Cookeville, TN, USA. He is currently a faculty member at Carleton University, Ottawa, ON, Canada, and an Associated Faculty member at the Université du Québec à Trois-Rivières, Trois-Rivières, QC, Canada. His scholarly work has produced more than 85 journal and conference publications. His research interests include adaptive and nonlinear control theory, intelligent control, robotics, electric motor drives, and energy storage devices.

Dr. Chaoui received the Best Thesis Award (health, natural science, and engineering) and the Governor General of Canada Gold Medal Award for his doctoral dissertation in 2012.

**Hamid Gualous** (M'14) was born in Morocco in 1967. He received the Ph.D. degree in electronics from the University Paris XI, Orsay, France, in 1994.

From 1996 to 2009, he was an Associate Professor in the FEMTO-ST Laboratory, University of Franche-Comte, Besançon, France. He is currently a Full Professor at the University of Caen-Basse Normandie, Caen, France, and the Director of LUSAC Laboratory. His main research interests include energy storage device, marine renewable energies, and energy management systems for smart grids.

**Jalal Sabor** received the Ph.D. degree in engineering science from the Institut National des Sciences Appliquées, Rouen, France, in 1995.

He is currently a Professor of industrial computer science at the Ecole Nationale Supérieure d'Arts & Métiers, Université Moulay Ismail, Meknes, Morocco. He is a member of the LSMI Laboratory, Meknes, Morocco, and is also the research team control steering and supervision systems head. His main research interests include intelligent management of energy, smart grid, control and supervision systems, architecture based on multi-agent systems, and fuzzy logic.